

Electrogenerated Chemiluminescence of the Ruthenium Tris(2,2')bipyridyl/Amines System on a Boron-Doped Diamond Electrode

K. Honda, M. Yoshimura, Tata N. Rao, and A. Fujishima*

Department of Applied Chemistry, School of Engineering, The University of Tokyo, 7-3-1 Hongo, Bunkyo-ku, Tokyo 113-8656, Japan

Received: October 7, 2002; In Final Form: December 7, 2002

The electrogenerated chemiluminescence (ECL) process of the $\text{Ru}(\text{bpy})_3^{2+}$ ($\text{bpy} = 2,2'$ -bipyridyl)/co-reactant system at an as-deposited diamond electrode was investigated using cyclic voltammetry (CV) and electrochemical impedance measurements. At an as-deposited diamond electrode, three ECL waves (1.2 V, 2.0 V, 2.3 V vs Ag/AgCl) for tripropylamine (TPrA) were obtained. The anodic potential limit for ECL emission at as-deposited diamond was 2.5 V vs Ag/AgCl due to its wide potential window in the aqueous solution. The potential range of ECL at diamond was much wider than those for glassy carbon (GC) and polycrystalline Pt electrodes, suggesting the possibility of the ECL for amines with higher oxidation potentials. For the ECL peaks at 1.2 V corresponding to the oxidation potential for $\text{Ru}(\text{bpy})_3^{2+}$, the current densities and light intensities were increased linearly with the square root of the TPrA concentration. This suggests that TPrA oxidation necessary for the ECL occurred thorough homogeneous electron transfer between $\text{Ru}(\text{bpy})_3^{3+}$ and TPrA species. However, for the ECL peaks at 1.9 V, the current densities and light intensities were increased linearly with an increase in TPrA concentration, suggesting that TPrA oxidation was due to direct oxidation at the electrode surface. At the direct TPrA oxidation potential, dealkylation was found to occur and produce the corresponding secondary amine, primary amine, and the appropriate aldehyde. The ECL peak for TPrA at 2.3 V was found to be the ECL for propylamine, generated by the dealkylation. By use of a diamond electrode, even for primary amines, i.e., methylamine (MeA) or ethylamine (EtA) with very high oxidation potentials, the direct oxidation potential could be detected through the ECL process. The behavior of the ECL of TPrA for the as-deposited diamond and GC electrodes was investigated by long-term (1000) potential cycling. For the as-deposited diamond electrode, the light intensity showed stable behavior during the entire cycle. The decrease of the light intensity was only ca. 0.1 of the initial intensity. The high stability for the as-deposited diamond was found to be attributable to the low adsorption property for reaction products on the diamond surface. We could show that the diamond electrode is the promising candidate for the electrode material for ECL with a wide ECL potential region and high stability.

Introduction

The boron-doped diamond thin film has emerged as an attractive electrode material due to its wide electrochemical potential window in aqueous^{1,2} and nonaqueous³ media and its extreme electrochemical stability.⁴ Recently, many potential applications of diamond electrodes have been published, including charge storage as an electrical double-layer capacitor,^{5–7} electrochemical treatment of wastewater,⁸ and electrosynthesis⁹ by making use of its characteristic properties. Moreover, diamond possesses morphological stability at extreme anodic and cathodic potentials and corrosion resistance in both acidic and alkaline conditions. Polycrystalline diamond is ideally suited as an electrocatalyst support for fuel cells.^{10–12}

In recent years, many reports were published about electroanalytical applications of diamond as it is thought to be an ideal electrode material for electroanalytical detection of biological species.^{13–15} However, the diamond electrode does not exhibit the electrocatalytic activity, i.e., methanol oxidation,¹⁶ and the selectivity for specific compounds is relatively low. Modification of the diamond electrode with various catalysts

and enzymes was attempted in order to improve the selectivity of diamond.¹⁷ By these treatments, ideal diamond characteristics, i.e., wide potential window and low background current, were partially lost. Therefore, it is necessary to develop a method for adding the selectivity to diamond without losing its superior characteristics.

For this purpose, the highly sensitive and selective detection, i.e., amines or ketones, using the electrogenerated chemiluminescence (ECL) is a promising analytical method to make use of the superiority of the diamond electrode without the requirement of modification.

Electrogenerated chemiluminescence using $\text{Ru}(\text{bpy})_3^{2+}$ has superior properties including high sensitivity and high stability under moderate conditions in aqueous solution.

Therefore, there have been many reports on the detection of various compounds using the ECL as the detector in the flow injection analysis.^{18,19} Rapid determination detection of the amino acid and peptide is important in terms of the evaluation for the activity as enzyme. The analytical method using ECL is the highly sensitive method for detecting the bio-related compound including the amino functional group. However, immunoassay using ECL which is already commercialized for this purpose is not a simple method because it needs long-term

* Corresponding author. Phone: 81 3 5841 7245. Fax: 81 3 3812 6227. E-mail: akira-fu@fchem.chem.t.u-tokyo.ac.jp.

preparation of the sample.²⁰ To develop the simpler electroanalytical system for amino acids, like electrochemical detection in HPLC, it is necessary to understand the mechanism of the Ru(bpy)₃²⁺/amines system and to invent a new ECL method to improve the selectivity and the sensitivity.

For GC and polycrystalline Pt electrodes, the ECL reaction process has been reported as a complicated process involving many intermediate reactions, because these electrodes have a relatively narrow ECL range and high activity for oxidation of the organic compound (i.e., TPrA). Boron-doped diamond exhibits the fast reaction rate for the charge-transfer reaction even at the high over-potential within the wide potential range. Moreover, this electrode has a different electrochemical activity for the oxidation of the organic compound in comparison to GC and polycrystalline Pt. Therefore, the complicated ECL process including several routes can be separated at the diamond surface. Also, by using the diamond electrode, the ECL in the high potentials is expected to be observable for compounds with high oxidation potential which is difficult to detect using GC or polycrystalline Pt electrodes with a limited working potential.

The objective of this study is to make clear the electrogenerated chemiluminescence process of the Ru(bpy)₃²⁺/amines system at an as-deposited diamond electrode by comparing it with those for other electrode materials. The separation of the different ECL route of the Ru(bpy)₃²⁺/amines system and the electrochemical detection of amines with higher oxidation potential are demonstrated. By using a diamond surface, we could show for the first time that the successive dealkylation reactions for amines are included in the ECL process. Furthermore, the possibility for analytical applications will be investigated.

Experimental Section

Highly boron-doped diamond films were deposited on n-Si(111) substrates using a high-pressure plasma-assisted chemical vapor deposition (CVD) system (ASTeX Corp., Woburn, MA). The resistivity of the Si substrate was ca. $5 \times 10^{-3} \Omega \text{ cm}$. Details of the deposition process have been reported elsewhere.²¹ B₂O₃ (Extra Pure, Wako Chemical Co., Ltd.) was used as the boron source. A 9:1 (v/v) mixture of acetone and methanol was used as the carbon source. B₂O₃ was dissolved in this solvent mixture so that the nominal B/C ratio (mol/mol) was 10⁴ ppm in the gas phase. The typical boron concentration obtained under these conditions is ca. $1.5 \times 10^{21} \text{ cm}^{-3}$.²² The resistivity of the resulting boron-doped diamond film was ca. $10^{-3} \Omega \text{ cm}$.

The as-deposited diamond film was used as electrodes without removal from the Si substrates. Ohmic contact was made from the back of the highly conductive Si substrates. A copper wire was attached using silver paste (Dotite D-550, Fujikura Kasei Co. Ltd., Japan). Both the contact area and the backside of the film were covered with epoxy (Araldite, Ciba-Geigy Co. Ltd., Switzerland). The resistivity of the boron-doped diamond film ($10^{-3} \Omega \text{ cm}$) was in the same range as that of the Si substrate. Therefore, there was no difference in the electrochemical behavior between the diamond film with which the ohmic contact was made from the backside of the Si substrate and that for the front side of the diamond films. The glassy carbon (GC, GC-20, Tokai Ltd.) electrode was prepared by polishing with successively finer grades of alumina powder slurried in ultrapure water (1.0, 0.3, and 0.05 μm) on a felt pad. The electrode was rinsed thoroughly and ultrasonicated in ultrapure water (15 min) after each polishing step. The polycrystalline Pt electrode was preactivated by scanning the potential in 1 M H₂SO₄ solution between 1.18 and -0.18 V vs Ag/AgCl at 50

mV s⁻¹ for 180 min. The maximum current density achieved at the anodic and cathodic potential limit was ca. 0.3 mA cm^{-2} (geometric area basis). By this pretreatment, the surface of the Pt metal is cleaned and activated.

The electrochemical measurements were carried out in a single-compartment, three-electrode glass cell with an Ag/AgCl (3 M KCl) reference electrode and platinum gauze counter electrode. All experiments were done at room temperature (23 °C). The electrode area was 0.071 cm². The ECL signal was measured with a photomultiplier tube (PMT, Hamamatsu R928) installed under the electrochemical cell. A voltage of 375 V was supplied to the PMT with a home-built high-voltage supply. The current density and the normalized ECL intensity (PMT output I_{ECL}) were calculated according to the geometric area of the electrodes.

Electrochemical measurements were carried out with the use of a potentiostat/galvanostat (Hokuto Denko Research, model HZ-3000). Cyclic voltammograms were obtained at a sweep rate of 50 mV s⁻¹. The AC impedance measurements (averaged over 10 cycles) were carried out at an amplitude of 10 mV (rms) in the frequency range from 100 kHz to 0.01 Hz with a potentiostat/galvanostat (model 2020, Toho Technical Research) and a frequency response analyzer (NF Electronic Instruments, model S-5720B). Complex impedance (Cole–Cole) plots were obtained at 1.2 and 1.9 V, which are within the potential ranges in which the ECL reaction was observed on the as-deposited diamond electrodes.

All chemicals were used without further purification. Ru(bpy)₃Cl₂·6H₂O (minimum 98%) was obtained from Aldrich (Milwaukee, WI). Tripropylamine, dipropylamine, propylamine, triethylamine, diethylamine, ethylamine, trimethylamine, dimethylamine, and methylamine were reagent grade quality (Wako, Japan). The amine was dissolved in 0.2 M phosphate buffer solution (PBS). The pH value of the solution was adjusted to 7.5 with NaOH or NaH₂PO₄. In aqueous Ru(bpy)₃²⁺ ECL analysis, the optimum pH value of the TPrA buffer solution is about 7–8, and the concentrated TPrA (around 100 mM) is usually used to achieve high ECL intensity.²³ The solutions were prepared in Milli-Q water (Millipore). The solutions were deoxygenated with nitrogen for 15 min prior to analysis.

Results and Discussion

1. Cyclic Voltammograms for ECL. 1.1. CV at the As-Deposited Diamond, GC, and Polycrystalline Pt Electrodes. The electrochemical behavior was investigated by use of cyclic voltammograms (CV). Figure 1 shows voltage–ECL curves of 300 μM Ru(bpy)₃²⁺ in 0.2 M phosphate buffer solution (pH 7.5) in the presence of 100 mM TPrA at as-deposited diamond, glassy carbon (GC), and polycrystalline Pt (Pt) electrodes.

As shown in Figure 1A, at the diamond electrode, light intensity started at $\sim 1.0 \text{ V}$, and three ECL waves appeared during the positive scan. The first ECL peak was observed at 1.30 V. Beyond 1.3 V, a plateau was formed and the second ECL peak was obtained at 1.89 V. The ECL intensity gradually decreased, and the third ECL wave appeared at 2.33 V as a shoulder. The anodic limit is ca. 2.5 V. The onset potential of the first ECL peak (1.0 V) corresponds to the potential of the oxidation potential for Ru(bpy)₃²⁺, as shown in Figure 1A. At the first ECL wave, the Ru(bpy)₃²⁺ may play an important role in the ECL process. The current density also, started at 1.0 V, formed a plateau from 1.3 to 1.8 V. The second voltammetric wave was obtained at the potential of ca. 1.8 V, the same potential as the second ECL peak. The ECL mechanism at the second peak is supposed to be closely related with direct oxidation of TPrA.

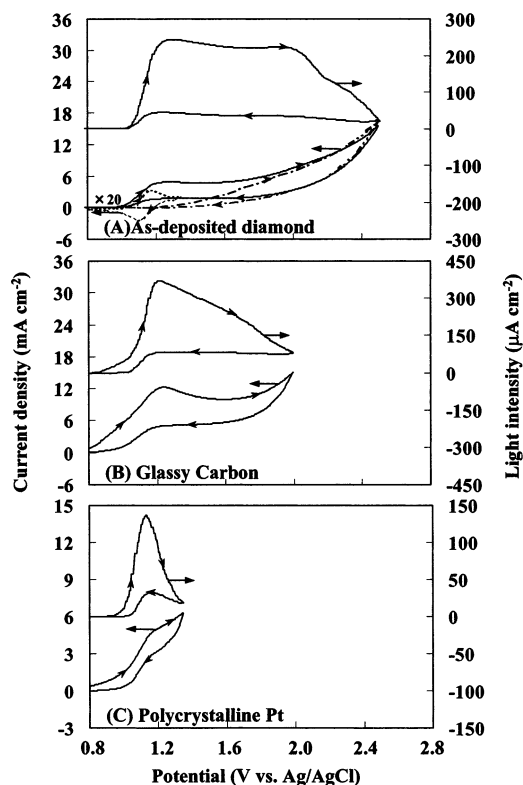


Figure 1. Cyclic voltammograms and ECL curves at (A) as-deposited diamond, (B) glassy carbon, and (C) polycrystalline Pt electrodes in 0.2 M phosphate buffer solution containing 300 μM $\text{Ru}(\text{bpy})_3^{2+}$ and 0.1 M TPrA. The dotted line represents data in the absence of TPrA. The dot-dashed line presents data in the absence of $\text{Ru}(\text{bpy})_3\text{Cl}_2$. Sweep rate: 50 mV s^{-1} , geometric area: 0.071 cm^2 .

Figure 1A shows that the anodic current for TPrA oxidation started at ca. 1.4 V and reached 5.0 mA cm^{-2} at 1.85 V, overlapping the CV curve of TPrA in the presence of $\text{Ru}(\text{bpy})_3^{2+}$ at these higher potentials. Therefore, this result indicates that at potentials over 1.85 V the anodic current for the mixture of TPrA and $\text{Ru}(\text{bpy})_3^{2+}$ could be mainly attributable to the current for the direct oxidation reaction of TPrA. In this study, the electrolyte solution includes Cl^- from $\text{Ru}(\text{bpy})_3\text{Cl}_2$. Hence, in Figure 1A, there is a possibility of a Cl_2 evolution reaction at high anodic potential regions. In a separate experiment, at the as-deposited diamond electrode, a chlorine evolution reaction was observed with oxygen evolution in the 0.1 M KCl. The anodic current onset was observed at ca. 1.7 V vs Ag/AgCl of that at the second ECL peak in Figure 1A. In Figure 1A, as the concentration of Cl^- was very low (0.3 mM), the contribution from the chlorine evolution should be as low as 0.01 mA cm^{-2} . This value was 1.5% of the total anodic current (7.58 mA cm^{-2}) observed in Figure 1A. Therefore, the effect of the chlorine evolution reaction for the ECL reaction was supposed to be quite low.

At the GC electrode (Figure 1B), it is a unique characteristic that the onset of the ECL wave is ca. 0.8 V, a potential that is too negative to generate $\text{Ru}(\text{bpy})_3^{3+}$. One ECL peak was observed at 1.22 V at positive scan, reaching the anodic limit of ca. 2.0 V. The limit for GC was lower by 0.5 V than that for as-deposited diamond. For the GC electrode, the ECL process might be different from that for the first ECL peak at diamond because of the different onset potential and higher current density at the ECL peaks (GC, 12 mA cm^{-2} ; diamond, 5 mA cm^{-2}).

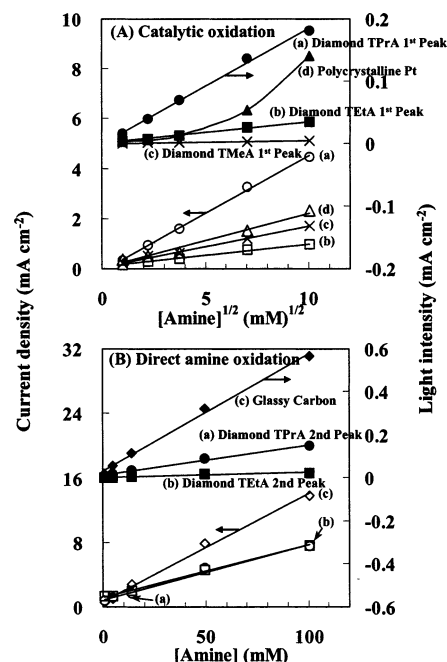


Figure 2. The dependence of the light intensities and the current densities on amine concentrations in voltage-ECL curves of Figure 1. (A) At the first ECL peak potential for (a) TPrA, (b) TEtA, and (c) TMeA at an as-deposited diamond electrode, and (d) TPrA at a polycrystalline Pt electrode. (B) At the second ECL peak potential for (a) TPrA, (b) TEtA, and (c) the ECL peak for TPrA at a GC electrode.

At the polycrystalline Pt electrode (Figure 1C), the onset of ECL (0.9 V) was near that for GC and only one ECL peak was obtained at 1.12 V at a positive scan. The ECL peak intensity for Pt was ca. 0.5 of that for as-deposited diamond. The anodic limit at Pt was 1.4 V, showing a small ECL emission range (ca. 0.5 V). The ECL emission range for as-deposited diamond is ca. 1.5 V and this is ca. 3 times wider than that for Pt. The ECL wave at such a high potential region has not been demonstrated in earlier studies. This is one of the unique properties of the diamond.

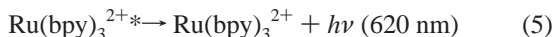
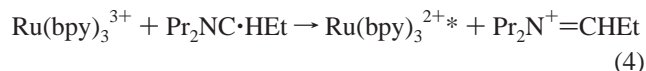
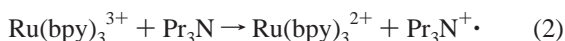
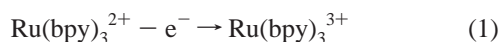
In Figure 1, at the GC electrode, the anodic current started at a lower potential than that for as-deposited diamond. It was reported at the GC electrode that TPrA direct oxidation started at ca. 0.6 V.²⁴ The fact that inner sphere redox species were relatively oxidized at high overpotential at the diamond electrode (as in the case of oxygen evolution) is the main reason for this higher potential value. In the case of a polycrystalline Pt electrode, it was reported that TPrA oxidation occurred at the potential regions of the electrochemical oxidation of the Pt surface (from 0.4 to 0.9 V).²⁴

The spectra of the ECL signal for as-deposited diamond were measured at three peak potentials (1.30, 1.86, and 2.33 V) with photonic multichannel analyzer (PMA-10, Hamamatsu). In all three spectra, the peaks of ECL emission were obtained at 610 nm, indicating that the light was emitted from the excited state of $\text{Ru}(\text{bpy})_3^{2+*}$.^{24,25} Therefore, the potential difference of three peaks suggests that the ECL process at each peak potential might include the different route to generate $\text{Ru}(\text{bpy})_3^{2+*}$. We will discuss the reaction route for each peak potential at the as-deposited diamond electrode.

1.2. ECL Route for the First Peak at As-Deposited Diamond. At first, we will discuss the ECL process at the first peak potential corresponding to the oxidation potential of $\text{Ru}(\text{bpy})_3^{2+}$. Figure 2 shows variation of the current densities and light intensities with the amine concentrations (1 mM–100 mM) in 300 mM $\text{Ru}(\text{bpy})_3^{2+}$ for as-deposited diamond, GC, and

polycrystalline Pt electrode. At the GC electrode (Figure 2B-c), both peak intensities depend linearly on the TPrA concentration. However, at as-deposited diamond (Figure 2A-a), light intensity and current density at the first peak were increased linearly with the square root of the amine concentration. In the case of variation with $\text{Ru}(\text{bpy})_3^{2+}$ concentration ($10\ \mu\text{M}$ – $300\ \mu\text{M}$) in $100\ \text{mM}$ TPrA (not shown), at both of the as-deposited diamond and GC electrodes, both peak intensities at $1.2\ \text{V}$ increase linearly with increasing Ru complex concentrations. Light intensity for as-deposited diamond and GC were in the same level, but the current densities for GC were a factor of 2 higher than that for as-deposited diamond. Then, the efficiencies of ECL (ratio of the light intensity and current density) for diamond were also a factor of 2 higher than those for GC.

In the $\text{Ru}(\text{bpy})_3^{2+}/\text{TPrA}$ system, the generation of the excited state ($\text{Ru}(\text{bpy})_3^{2+*}$) has been explained as being generated from the reaction between the highly reducing radical species $\text{Pr}_2\text{NC}\cdot\text{HEt}$ and $\text{Ru}(\text{bpy})_3^{3+}$. The free radical $\text{Pr}_2\text{NC}\cdot\text{HEt}$ was formed by the deprotonation of the TPrA radical cation ($\text{Pr}_3\text{N}^+\cdot$) resulting from oxidizing TPrA. In a previous publication, two routes to form $\text{Pr}_3\text{N}^+\cdot$ have been reported. One of these routes is called the catalytic route. In this route, the oxidation of TPrA occurs through the homogeneous electron-transfer reaction with electrogenerated $\text{Ru}(\text{bpy})_3^{3+}$.²⁴ The reactions can be expressed by



In the first ECL peak at a diamond electrode, as the onset potential of ECL was equal to the potential for generating $\text{Ru}(\text{bpy})_3^{3+}$ and the current densities depend on the square root of the amine concentration, TPrA oxidation reaction is supposed to be due to the homogeneous reaction (eq 2).

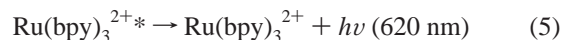
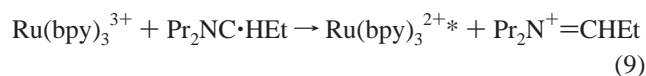
For an irreversible catalytic reaction following a reversible charge-transfer reaction, like eqs 1 and 2, the theory of stationary electrode polarography for CV has been treated by Nicholson and Shain.²⁵ According to this theory, for the large value of k_f/a (k_f is the rate constant of reaction 2 and a is the parameter related to the scan rate v , $a = nFv/RT$), the equation describing current–voltage–concentration relationships is

$$i = \frac{nFA\sqrt{Dk_fC_O^*}}{1 + \exp\left[\frac{nF}{RT}(E - E_{1/2})\right]} \quad (6)$$

where A is the electrode area, and D and C_O^* are the diffusion coefficient and bulk concentration of $\text{Ru}(\text{bpy})_3^{2+}$, respectively. $E_{1/2}$ is the polarographic half wave potential. For the very cathodic potentials, eq 6 reduces to $i = nFAC_O^*\sqrt{Dk_f}$, suggesting the characteristic flat limiting current region.²⁶ Since $k_f = k[\text{TPrA}]$, the current should be proportional to $\sqrt{[\text{TPrA}]}$, and a plot of the current as a function of $\sqrt{[\text{TPrA}]}$ should be linear, with a slope proportional to $\sqrt{k_f}$. In Figure 1A, the characteristic flat limiting current²⁶ was observed as a plateau region

from $1.3\ \text{V}$ to $1.8\ \text{V}$. Moreover, in Figure 2A-a, the current density of the first ECL peak potential exhibits the linear relation with the square root of the TPrA concentration. Therefore, we could conclude that the ECL process at the first peak is assigned to the catalytic route.

1.3. ECL Route for the Second Peak at As-Deposited Diamond. For a GC electrode, as shown in Figure 2B-c, the current densities and light intensities at ECL peak increased linearly with increasing TPrA concentration. Another route to produce $\text{Pr}_3\text{N}^+\cdot$ is the direct TPrA oxidation at the electrode surface (direct oxidation route). The mechanism proposed for this route is²⁴



In a previous report, the mechanism of the ECL peak at $1.22\ \text{V}$ for GC was described as the combination of the catalytic route and the direct oxidation route, and the direct oxidation route plays the dominant role at $\text{Ru}(\text{bpy})_3^{2+}$ concentrations under $0.5\ \text{mM}$.²⁴

Figure 2B-a shows the TPrA concentration dependence of the second ECL peaks at an as-deposited diamond electrode. The current densities and the light intensities increased linearly with increasing TPrA concentration. In the case of dependence on $\text{Ru}(\text{bpy})_3^{2+}$ concentration ($10\ \mu\text{M}$ – $300\ \mu\text{M}$) in $0.1\ \text{M}$ TPrA, the light intensities increased linearly, but the current densities were almost constant (not shown). This behavior of peak intensity is the same as that for a GC electrode, indicating that the TPrA oxidation occurs through the direct oxidation reaction at the electrode surface. Therefore, the second ECL peak potential can be mainly assigned as the oxidation potential of TPrA at as-deposited diamond.

The ECL process at polycrystalline Pt electrode also involved both the catalytic and direct oxidation of TPrA.^{23,24} However, since direct TPrA oxidation was inhibited by the surface oxide and the direct oxidation rate of TPrA was relatively low, the contribution of the direct oxidation route to the ECL process was reported to be small. In our result, as shown in Figure 2A-d, the dominant ECL process changed with the amine concentration. In the case of the higher concentration ($>5\ \text{mM}$) of TPrA, the light intensities depend linearly on the amine concentration, the same as that for GC. But, in the lower region ($<5\ \text{mM}$), the light intensity depends linearly on the square root of the amine concentration as the first ECL peak at as-deposited diamond.

The ECL mechanism at high over-potential like the third ECL shoulder at as-deposited diamond has not been reported. However, there are many reports that in electrochemical direct oxidation of tripropylamine, the successive dealkylation occurs to produce dipropylamine and propylamine.^{28–30}

The third ECL shoulder obtained at as-deposited diamond was supposed to be due to the ECL reaction through the direct oxidation for the dealkylation products. The secondary and primary amines are supposed to undergo oxidation at higher potential than a tertiary amine. To clarify this supposition, the

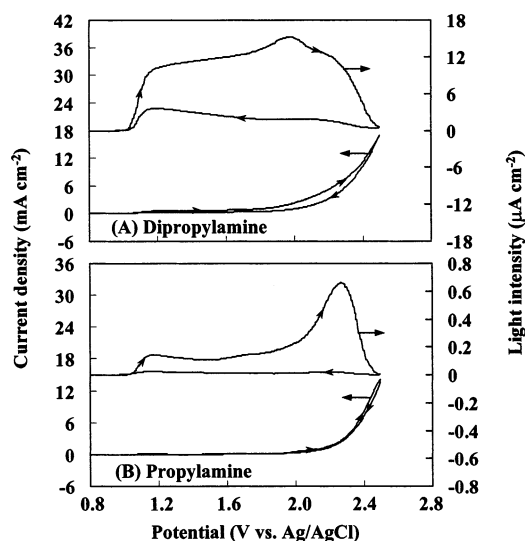


Figure 3. Cyclic voltammograms and ECL curves at the as-deposited diamond electrodes in 0.2 M phosphate buffer solution containing 300 μM $\text{Ru}(\text{bpy})_3^{2+}$ and 0.1 M (A) DPrA and (B) PrA. Sweep rate: 50 mV s^{-1} , geometric area: 0.071 cm^2 .

TABLE 1: Comparison of the Peak Potential and Light Intensities in Figures 1, 2, 3, and 4 for Various Amines at the As-Deposited Diamond Electrode

peak	potential V	light intensity $\mu\text{A cm}^{-2}$	potential V	light intensity $\mu\text{A cm}^{-2}$	potential V	light intensity $\mu\text{A cm}^{-2}$
1 TPrA			2 DPrA		3 PrA	
1st	1.30	244	1.22	10.4	1.18	0.145
2nd	1.86	222	1.98	15.2	2.27	0.661
3rd	2.33	99	2.28	10.3		
4 TEtA			5 DEtA		6 EtA	
1st	1.20	29.1	1.21	1.36	1.18	0.082
2nd	1.91	73.5	2.24	5.54	2.26	0.402
3rd	2.25	39.7				
7 TMeA			8 DMeA		9 MeA	
1st	1.245	6.05	1.20	0.68	1.17	0.024
2nd	2.04	9.47	2.24	2.51	2.25	0.186
3rd	2.22	10.4				

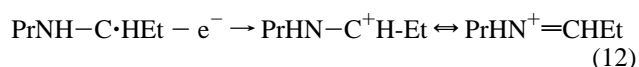
comparison of the ECL behavior of tertiary amine and that for secondary and primary amines as co-reactant was carried out.

1.4. ECL Route for the Third Shoulder at As-Deposited Diamond. Figure 3 shows voltage–ECL curves for dipropylamine (DPrA) and propylamine (PrA) as co-reactants at an as-deposited diamond electrode. For DPrA, three ECL waves appeared during the positive scan at 1.22 V, 1.98 V, and 2.28 V; for PrA, two waves (1.18 V and 2.27 V) were obtained. The peak potentials and the ECL intensities are summarized in Table 1.

The current densities for both amines started at ca. 1.0 V and exhibited the following plateaus. At the highest potentials, the current densities exhibited a second wave due to direct amine oxidations at the electrode surface. The onset potential for this amine direct oxidation shifted to a more positive potential with a decreasing number of alkyl groups. The potentials at which the current densities exceed 6 mA cm^{-2} for tripropylamine, dipropylamine, and propylamine were 1.82 V, 2.23 V, and 2.36 V, respectively. These results suggest that the oxidation potential of amine increases with decreasing the class. The first ECL peaks at ca. 1.2 V for both amines are attributable to the ECL through a catalytic route (eqs 1–5) similar to the first peak for TPrA. For PrA, the second ECL peak at 2.27 V is also the same as the onset of the second voltammetric wave. Therefore, the

second ECL process for PrA is attributable to the direct oxidation route similar to the ECL for GC (eqs 7–9).

In Figure 3A, the peak potential of the third ECL shoulder (2.36 V) for DPrA is close to the potential for the second ECL peak for PrA, suggesting that the ECL of this peak is the direct oxidation peak for PrA generated by the dealkylation of DPrA. For DPrA, the second ECL peak potential was the same as the onset of the second voltammetric wave. Therefore, it was supposed that at the second peak potential, the ECL reaction through the direct oxidation of DPrA (the same as eqs 7–9) and the generation of PrA through the dealkylation process were occurring simultaneously. The scheme of the dealkylation reaction can be expressed by



It was clarified that the ECL process for the higher class of amine include the dealkylation reaction in the direct oxidation route.

For TPrA, at the second ECL peak (1.86 V), the ECL of TPrA direct oxidation, and the generation of DPrA were supposed to occur simultaneously. Moreover, at the same potential region (1.98 V), the electrochemical reactions were attributable to the direct oxidation ECL of DPrA and the dealkylation of the DPrA, followed by the ECL through the direct oxidation of PrA at the third shoulder (2.33 V).

The peak potential for the second ECL in Figure 1A (TPrA) was relatively near that for the second ECL in Figure 3A (DPrA). One possible explanation is that at the second ECL potential in Figure 1A, the direct oxidation of TPrA and DPrA occurred successively. This is because the second ECL peak for TPrA occurs at the same potential, where a broad oxidation peak in the voltammogram appeared. Furthermore, the second ECL peak in Figure 1A is much broader than that for DPrA (Figure 3A), indicating that the peaks for TPrA and DPrA overlap. Hence, successive oxidation of TPrA and DPrA was suggested.

In addition, from Figure 3B, it was also assured that at the as-deposited diamond electrode, the oxidation potential of a primary amine with a very high oxidation potential could be detected. This is another advantage of the diamond electrode at the analytical ECL application. To clarify the possibility of detecting the amines with a higher oxidation potential, the ECL behavior for amines with smaller alkyl chains (i.e., ethyl- and methyl-) were examined.

1.5. ECL Behavior for Ethylamines and Methylamines at As-Deposited Diamond. As discussed in a previous section, at the diamond electrode with wide potential window, the oxidation potential could be detected using an ECL reaction for the organic compound which could not be observed at conventional electrode (i.e., GC and Pt) due to a higher oxidation potential than the anodic limit (oxygen evolution).

Figure 4 shows voltage–ECL curves of 300 mM $\text{Ru}(\text{bpy})_3^{2+}$ in 0.2 M phosphate buffer solution (pH 7.8) in the presence of 100 mM ethylamines and methylamines at as-deposited diamond. As shown in Figure 4A, for triethylamine (TEtA) also, the three ECL waves were obtained at a positive sweep similar

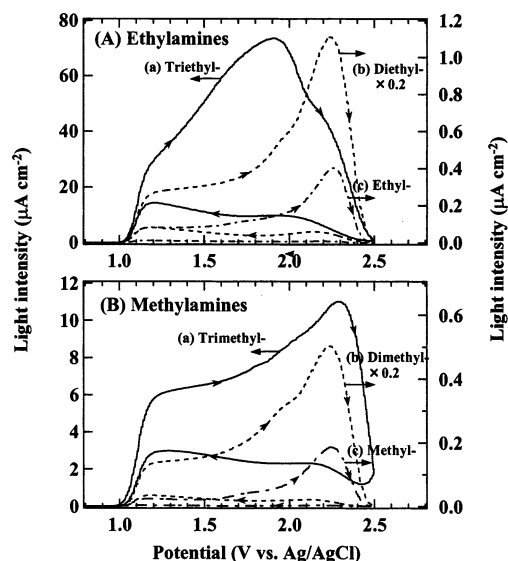


Figure 4. The ECL curves for (A) ethylamines and (B) methylamines at an as-deposited diamond electrode in 0.2 M phosphate buffer solution containing 300 μM $\text{Ru}(\text{bpy})_3^{2+}$ and 0.1 M amines: (a) tertiary amine (solid line), (b) secondary amine (dotted line), and (c) primary amine (dot-dashed line). Sweep rate: 50 mV s^{-1} , geometric area: 0.071 cm^2 .

to that for TPrA, and for diethylamine (DEtA) and ethylamine (EtA), two ECL waves were observed within the same potential range. The values of the ECL peaks and light intensities for all amines are summarized in Table 1. The first ECL peaks for all three ethylamines were consistent with that for TPrA, and its mechanism can be described as catalytic route (eqs 1–5).

The third ECL potential (2.25 V) for TEtA was equal to the potentials of the second peaks for DEtA and EtA. Therefore, the ECL reaction through the direct TEtA oxidation at 1.91 V was supposed to include the dealkylation reaction to produce DEtA. Three kinds of electrochemical reactions might be possible at this third ECL potential. These reactions are the ECL reaction and the dealkylation reaction for the DEtA generated at the second peak (1.91 V) and the ECL reaction for EtA. The separation of the ECL process for TEtA and the detection of the oxidation potential of the EtA were also successful. There are some small ECL peaks around 1.9 V in curve b of Figure 4A and 4B. In this study, the amines were of reagent grade quality (min. 99.0%) and used without further purification. Therefore, the amines included impurities up to 1.0%. The small ECL peaks at ca. 1.9 V in curve b of Figure 4A and 4B are possibly due to the impurities with low oxidation potential like tertiary amines.

For all three methylamines, only two ECL waves were observed, and each potential for the first and second ECL peaks was almost the same. The first ECL peak for all methylamines was also consistent with that for TPrA, indicating the catalytic ECL route (eqs 1–5). In the case of TMeA, the separation of the ECL process using as-deposited diamond was not so effective. But, we surmise that at the second ECL peak potential, the ECL reaction and the dealkylation reaction due to direct oxidation for TMeA, DMeA, and MeA occur. Moreover, the detection of the oxidation potential even for methylamine with the highest oxidation potential was successful using ECL. For methylamine, the light intensity of the second ECL peak was ca. 7.8 times higher than that for the first peak. Therefore, by use of the second ECL process obtained only at the as-deposited diamond, the lower ECL detection limit for MeA can be increased by a factor of 10.¹⁸

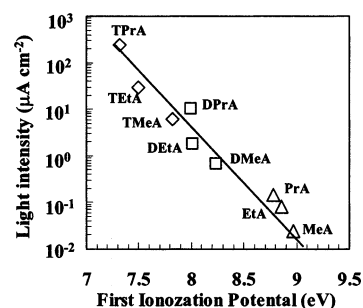


Figure 5. Plot of the log of the first ECL peak intensity against the aliphatic amine's first ionization potential. The aliphatic amines belong to the following classes: propylamines (\diamond); ethylamines (\square); methylamines (\triangle).

As shown in Figure 2, for both TEtA and TMeA, the current densities and light intensities for the first ECL peak increased linearly with the square root of the amine concentrations, and those for the second peaks depend linearly on the amine concentrations. This result also supports the ECL mechanism at the first peak for these amines, described above.

The comparison of the ECL intensity for each amine was carried out. Figure 5 shows a plot of the log of the ECL light intensity at the first ECL peak potential for the aliphatic amines versus the energy of their first ionization potential. The values for first ionization potentials were used from the literature.³¹ In Figure 5, the light intensity of alkylamines increases in the order tertiary > secondary > primary. The magnitude of light intensity decreases with decreasing alkyl chain length within each class i.e., primary, secondary, and tertiary amines. This tendency is consistent with the difficulty of the electrochemical oxidation of amines at the Pt electrode.²⁸ This is because the alkyl groups are more strongly electron donating than hydrogen atoms. Then, a decrease in alkyl groups (increase in hydrogen atoms) should make the electrons of the nitrogen less available for the oxidation reaction of amines. Similarly, with increasing carbon atoms in the alkyl chain, the electron donating to the nitrogen atom becomes higher, with the result that the electrons of the nitrogen are easily available for oxidation. The difficulty of the oxidation in the catalytic ECL process in that $\text{Ru}(\text{bpy})_3^{2+}$ acts as a mediator also supposed to be affected by this substituent effect.

As shown in Figure 5, the linear relationship existed between the log of the ECL peak intensity and ionization potential of the amine. The correlation coefficient for this plot was 0.954. This correlation is reasonable for the chemically similar compounds with an endergonic or exergonic electron transfer reaction. And this tendency is consistent with results reported by Noffsinger and Danielson using the ECL from the mixture of $\text{Ru}(\text{bpy})_3^{3+}$ and amines.¹⁸ This linear relation also supports the supposition of the ECL mechanism at the first peak.

For the second ECL peak, the variation of the light intensity has almost the same tendency as that for the first peak described above (Table 1). The intensity for TPrA has the maximum value, which is 1000 times higher than the maximum value for MeA. Moreover, the order of the oxidation potentials obtained using ECL was consistent with the direct oxidation potentials for aliphatic amines obtained at the Pt electrode in acetonitrile solution.²⁸ However, the reported values for TPrA, DPrA, and PrA at Pt were 1.15 V, 1.25 V, and 1.62 V vs NHE, respectively.²⁸ The ECL values obtained in this study are higher by ca. 0.8 V than those obtained at Pt. The difference between our results and the reported values might be due to the difference in pH and surface conditions. It has been reported that the oxidation potential for TPrA has increased from 0.92 to 1.4 V vs NHE with decreasing pH from 12.3 to 7 at the GC

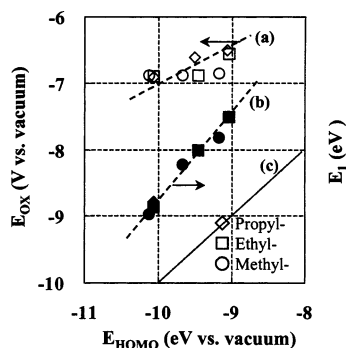


Figure 6. Correlation of HOMO energies of aliphatic amines calculated by the HF methods with (a) the oxidation potentials observed for the second ECL peaks, and (b) the first ionization potential. The aliphatic amines belong to the following classes: propylamines (\diamond); ethylamines (\square); methylamines (\triangle).

electrode.³² Furthermore, the value (1.15 V vs NHE) reported for GC at pH 9 is different from our value obtained at pH 7.5 due to the difference in pH. Another possibility is the difference in the electrochemical activity at the electrode surface for amine oxidation between GC, Pt, and the as-deposited diamond electrodes. It has been reported that for the oxidation polyamines in the low potential region (1.0 V vs SCE), nondiamond carbon impurities were necessary for the diamond surface to generate a reactive OH radical which plays a dominant role in the direct polyamine oxidation, suggesting that at a high quality diamond surface, the activity for amine oxidation is relatively low.³³ In the present study, as the high quality diamond without nondiamond impurities was used, a higher applied potential was required for the oxidation of amines. The reaction process for direct TPrA oxidation obtained for ECL may be different from the reaction process for the oxidation of polyamines on the diamond with nondiamond impurities.³³

Among these previous publications, there are few examples about the detection for the primary amine with higher oxidation potential such as MeA. The electrochemical observation for the oxidation peak of MeA is realized for the first time by use of the diamond electrode.

The measured oxidation potentials at the second ECL peak were supposed to be similar to the formation potential of the aminium cation radical $\text{Pr}_3\text{N}^{+\bullet}$ (eq 10) at the diamond electrode.²⁹ This first step of oxidation results from the outer-sphere electron transfer from amines. In outer-sphere electron transfer, the electron transfers efficiently just when the electrode potential is close to the HOMO and LUMO energies of the reactant molecule.³⁴ In this case, the initial product of oxidation is the radical cation. Thus far, we have attempted to check the correlation between the oxidation potentials and the highest occupied molecular orbital (HOMO) energies for the amines in order to ensure the mechanistic scheme of the oxidation reaction. Figure 6 presents the correlation between the calculated HOMO energies obtained from the HF technique and the second ECL peak potentials at the diamond electrode. The oxidation potentials in the voltage–ECL curves were converted into the absolute potentials (E_{abs}) using the formula E_{abs} (V vs vacuum) = $-E$ (V vs SHE) – 4.44.³⁵ Minus values of the first ionization potential (E_1) for aliphatic amines³¹ were also shown in Figure 6. First ionization potentials were equal to the energy for withdrawing the electron from the HOMO; thus far the correlation between the E_1 values and HOMO energies is reasonable, with the correlation coefficient (the slope of the correlation curve) of 1.42 V/eV, which is close to unity.

According to previous reports,^{36,37} the potentials (E_{ox}) for oxidation of an organic molecule with respect to vacuum are

related to the HOMO energy (E_{HOMO}) by the following equation:

$$E_{\text{HOMO}} = E_{\text{ox}} - \Delta E_{\text{sol}} + \text{const} \quad (14)$$

where ΔE_{sol} is the difference in the solvation energies of the neutral molecule and cation radical.^{37–39} An additional effect is that the HOMO energy level changes upon ionization due to changes in electron interactions, including correlation and repulsion. Ignoring the effect of the solvation and electron interaction, one-to-one correspondence between E_{ox} and E_{HOMO} was expected and a straight correlation line was produced with a slope of 1 V/eV (Figure 6).

The $E_{\text{HOMO}} - E_{\text{ox}}$ values obtained from the second ECL peaks are located by ca. 2.5 V over curve b, which may be due to the effect of solvation and electron interaction.³⁶ The slope of the least-squares fit to the data is 0.58 V/eV, which is relatively smaller than the ideal value (1 V/eV) for curve c.^{37,40} The deviation from the ideal slope was large at lower HOMO energy (the higher potential region). The reason for this large deviation is mainly due to the anodic potential limit for the diamond electrode. For methylamines the oxidation potentials measured by ECL were all observed at 2.3 V, as described before. These peaks might be formed at lower potentials due to quenching of $\text{Ru}(\text{bpy})_3^{2+\bullet}$ by O_2 generated at the anodic potential limit. Therefore, the degradation for the oxidation potentials at the potential limit causes the decline of the slope of the correlation curve.

In any case, a significant correlation (shown in eq 14) was obtained for the E_{ox} and E_{HOMO} results. Thus, it was confirmed that the second ECL peak potentials were attributable to the cation radical formation that results from outer-sphere electron transfer from amines.

2. Impedance Measurements for ECL. 2.1. Impedance Plots. The direct oxidation process for the as-deposited diamond is supposed to be the same as that for GC. But, the difference of the potential observed between as-deposited diamond and GC suggests that there is a difference of the electrochemical activity for direct TPrA oxidation. To confirm this difference of activity between the as-deposited diamond and GC, additional analysis using ac impedance behavior was carried out. The ac impedance measurements for as-deposited diamond, GC, and polycrystalline Pt electrodes during ECL reactions were carried out at the peak potentials obtained in the CV measurements (Figure 7A,B). The impedance plots for the as-deposited diamond (Figure 7A-a) at the first ECL peak and the polycrystalline Pt (Figure 7A-b) electrode consist of a combination of semicircles and a linear portion at a ca. 45-degree angle, which can be described by mass transport plus kinetic control. For both electrodes, the diameter of the semicircles decreases with an increase in the $\text{Ru}(\text{bpy})_3^{2+}$ concentration (not shown). The charge transfer reaction was mainly related to the $\text{Ru}(\text{bpy})_3^{2+}$ oxidation reaction. In contrast, the plots for the as-deposited diamond at the second ECL peak potential and the GC electrodes were composed of two depressed semicircles. The depression for the first semicircle at higher frequencies for the GC electrode was caused by the rotation in the counterclockwise direction around the origin by ca. 30 degrees.⁴¹ The diameter for both deformed semicircles was constant with an increase in the $\text{Ru}(\text{bpy})_3^{2+}$ concentration in 0.1 M TPrA (not shown), suggesting that the charge transfer reaction was mainly contributed from the oxidation reaction of TPrA, the oxidation of the electrode surface itself, or the oxygen evolution reaction. The diameter of the first semicircle in higher frequencies decreased with an increase in the observed potential from 1.9 V to 2.4 V, resulting in the decrease of the reaction resistance from 74 $\Omega \text{ cm}^2$ to 18

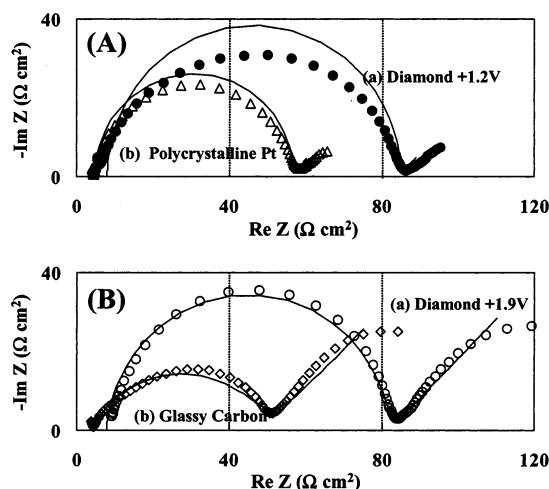


Figure 7. Impedance plots of the ECL reaction: (A) the ECL peak at 1.2 V vs Ag/AgCl for (a) the as-deposited diamond electrode, and (b) the polycrystalline Pt electrode; (B) the ECL peaks at (a) 1.9 V vs Ag/AgCl for the as-deposited diamond electrode, and (b) 1.2 V vs Ag/AgCl for the GC electrode. Experimental data points are shown as symbols for (●) at 1.2 V and (○) at 1.9 V on as-deposited diamond, (△) polycrystalline Pt, and (◇) GC. The simulated curves, calculated on the basis of the equivalent circuit described in the text, are shown as solid lines. The parameters are summarized in Table 2.

$\Omega \text{ cm}^2$. This behavior is consistent with the increase in the current density from 6.5 mA cm^{-2} to 13.1 mA cm^{-2} in the same potential region due to direct oxidation of TPrA in CV measurement. Thus far, the first semicircle is most likely related to direct oxidation of TPrA at the electrode surface. The second semicircle in lower frequencies was not so sensitive for the measurement potential, indicating that the reaction rate of the second semicircle was very slow and has a small contribution to the anodic current. It might be due to the surface oxidation in this potential region.

At a polycrystalline Pt electrode, the ECL process has been reported to involve both the catalytic and direct oxidation of TPrA.^{23,24} However, this impedance result (Figure 7A) suggests that the ECL process for Pt was mainly contributed from the catalytic route similar to the as-deposited diamond. By the surface oxide layer, the direct oxidation rate of TPrA decreases in magnitude, and the contribution from the catalytic oxidation might increase.

2.2. Numerical Simulations. To estimate the reaction parameters for each ECL process, the numerical simulations using equivalent circuits were carried out. Detailed information concerning the explicit frequency dependence of the impedance results can be obtained by use of the Bode-type representation. Figure 8 shows experimental Bode plots for the as-deposited diamond, GC, and polycrystalline Pt electrodes. In this representation, pure resistances (R) appear as horizontal lines in the amplitude plots, with a phase angle of 0° , and pure capacitances (C) appear as lines with a slope of -1 in the amplitude plots, with a phase angle of -90° . For the first ECL peak at as-deposited diamond and the ECL at polycrystalline Pt, the frequency characteristics in the Bode plots exhibit R-C-R type behavior. Therefore, these impedances for ECL reaction can be simulated as a simple Randles equivalent circuit comprising a parallel combination of a double layer capacitance (C_d) and a semi-infinite Warburg impedance (Z_W ; characterized by the diffusion resistance δ) in series with a charge-transfer resistance (R_{CT}), which can be described by mass transport-controlled kinetics. The simulation curves are shown in Figures 7A and 8. Table 2 summarizes the values of the fitting parameters and

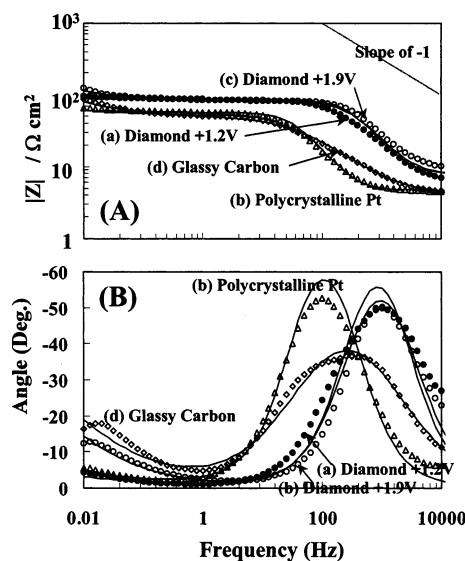


Figure 8. Bode amplitude (A) and phase angle (B) plots for the ECL reaction with TPrA: (a) the first ECL peak at 1.2 V vs Ag/AgCl at the as-deposited diamond; (b) the ECL peak at 1.2 V vs Ag/AgCl at the polycrystalline Pt electrode; (c) the second ECL peak at 1.9 V vs Ag/AgCl at the as-deposited diamond; and (d) the ECL peak at 1.2 V vs Ag/AgCl at the GC electrode. Experimental data points are shown as symbols for (●) at 1.2 V and (○) at 1.9 V on as-deposited diamond, (△) polycrystalline Pt, and (◇) GC. The simulated curves, calculated on the basis of the equivalent circuit described in the text, are shown as solid lines. The parameters are summarized in Table 2.

the average relative errors for the calculated curves. The fitting parameters shown are with respect to the geometric area. By use of both the impedance and Bode plots, we were able to reproduce the frequency behavior of the measured results. The fits are reasonably good, with the relative error of 11.3 and 9.5% for as-deposited diamond and polycrystalline Pt, respectively. For polycrystalline Pt, the C_d value is a factor of 10 larger than that for diamond, the result being that the peaks of the C_d element in the Bode phase angle plots (Figure 8B) shifted to ca. 100 Hz compared to that for the as-deposited diamond (ca. 1 kHz). In contrast, the R_{CT} values for both the as-deposited diamond and polycrystalline Pt are in the same range (76 and $51 \Omega \text{ cm}^2$, respectively), which is consistent with the current densities for both electrodes (ca. 6 mA cm^{-2}) in the CV measurements (Figure 1A,C). The δ values are also the same levels (2.4 and $2.3 \Omega \text{ cm}^2$), suggesting that the reactant molecule controlled by mass transfer is found to be the same.

In contrast, in the Bode plots for both the second ECL peak for the as-deposited diamond (Figure 8) and GC electrodes, there are differences in the lower frequencies ($< 1 \text{ Hz}$). In both cases, the amplitude and phase angle plots increased with decreasing frequency, forming the peaks at 0.05 Hz in phase angle plots. This peak at 0.05 Hz in the Bode phase angle plots corresponds to the second semicircle in the impedance plots (Figure 7B), resulting from the electrochemical reaction with slow reaction rate like an oxidation reaction of the electrode surface. In this paper, to reproduce these characteristics in the low-frequency range, the constant phase element (CPE) was introduced in the simple Randles circuit instead of the double layer capacitance. This component can describe a model of distributed time constants. The following equation was used as an equivalent circuit, and a nonlinear fit routine was carried out;

$$Z(j\omega) = R_s + \{[CPE] + (R_{CT} + Z_W)^{-1}\}^{-1} \quad (15)$$

where $\omega = 2\pi f$, and the constant phase element (CPE) includes

TABLE 2: Parameters Used for Fitting the Impedance Results for the ECL Reaction at As-Deposited Diamond, Polycrystalline Pt, and Glassy Carbon Electrodes in the Complex Plane Plots (Figures 7 and 8)

electrode	series resistance, R_s , $\Omega \text{ cm}^2$	differential capacitance, C_d , $\mu\text{F cm}^{-2}$	constant phase element, α	reaction resistance, R_{CT} , $\Omega \text{ cm}^2$	diffusion resistance, δ , $\Omega \text{ cm}^2$	average relative error
1st ECL peak at as-deposited diamond	8.0×10^0	8.0×10^0		7.6×10^1	2.4×10^0	11.3%
2nd ECL peak at as-deposited diamond	8.9×10^0	4.5×10^0	9.9×10^{-1}	4.9×10^1	7.1×10^0	8.69%
polycrystalline Pt	4.7×10^0	1.0×10^2		5.1×10^1	2.3×10^0	9.47%
glassy carbon	3.9×10^0	3.1×10^1	7.0×10^{-1}	4.6×10^1	6.4×10^0	5.45%

the double layer capacitance C_d and the power factor α , and is expressed by the following equation: $[CPE] = [C_d(j\omega)^\alpha]^{-1}$. It was supposed that such a distribution might arise from two causes. One is a microscopic roughness on the electrode surface caused by scratches and pits, always present on solid surfaces, which cause coupling of the solution resistance with the surface capacitance.⁴² Another is a capacitance dispersion of interfacial origin, connected with the slow adsorptions of ions and chemical inhomogeneities of the surface.⁴³ The CPE has been employed to reproduce the experimental results in the direct oxidation process for amines, i.e., the generation of the aniline monomer in the process of the formation of poly-aniline on the polycrystalline Pt electrode,⁴⁴ and the electrochemical oxidation of epinephrine on the GC electrode.⁴¹

By using this equivalent circuit and the parameters (Table 2), the calculated impedance plots could reproduce the experimental results. The relative average error for the second ECL peaks at diamond and GC electrodes were 4.9% and 5.5%, respectively. The R_{CT} and the δ values for the second peak at diamond and the peak at GC were in the same range, indicating that both charge-transfer reactions for ECL are the same process, as described in eqs 7–9.

In Figure 8, for a GC electrode, the capacitance peak in phase angle plots (Figure 8B) was also observed in lower frequencies than that for the diamond due to the larger C_d value ($31 \mu\text{F cm}^{-2}$, $4.5 \mu\text{F cm}^{-2}$ for the as-deposited diamond). Moreover, the α value for the GC and as-deposited diamond were 0.70 and 0.98, respectively. This parameter represents the degree of rotation around the origin in impedance plots (Figure 7B). This result suggests that there was no rotation for as-deposited diamond, but for the GC electrode, the α value was close to that in the oxidation process for epinephrine ($\alpha = 0.71$).⁴¹ The CPE behavior has been explained by two possible explanations described above: the microscopic roughening and the inhomogeneous distribution of the capacitance on the electrode surface. As the as-deposited diamond was composed from microcrystals of the range 3–10 μm , the microstructural roughness was greater than that of GC, then the larger α value at GC was mainly contributed by the inhomogeneous capacitance dispersion. However, the ECL reactions were supposed to be the same for both surfaces in terms of the CV results and measurements and the R_{CT} and δ values in the impedance results. Therefore, the low uniformity of capacitance dispersion might be due to the adsorption of the reaction products (oxidized forms of TPrA) on the electrode surface.

By use of the impedance measurements, the identity of the ECL process of the second peak at diamond and the ECL peak at GC was confirmed. In contrast, the difference of the degree of the adsorption for the reaction products between the as-deposited diamond and GC was also clarified. This difference was supposed to significantly affect the stability of the ECL at both electrodes. Therefore, in the next section, the stability of the ECL reaction was examined at these electrodes.

3. Potential Cycling for the ECL Reaction. In its application to the detection in the flow injection analysis (FIA) using the

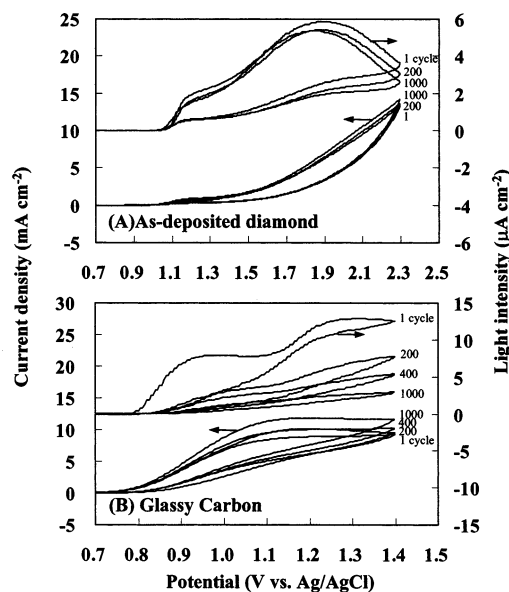


Figure 9. Voltage–ECL curves for (A) as-deposited diamond and (B) glassy carbon electrodes in 0.2 M phosphate buffer solution containing $10 \mu\text{M Ru}(\text{bpy})_3^{2+}$ and 0.1 M TPrA during 1000 potential cycles. Sweep rate: 50 mV s^{-1} , geometric area: 0.071 cm^2 .

boron-doped diamond and the $\text{Ru}(\text{bpy})_3^{3+}$, chemiluminescent stability of the ECL reaction is important. The behavior of ECL in the $\text{Ru}(\text{bpy})_3^{2+}$ /TPrA system for as-deposited diamond, GC, and polycrystalline Pt electrodes was investigated by the long-term potential cycling between 0 and 1.45 V over the ECL peak potential vs Ag/AgCl in 0.2 M phosphate buffer solution. For the as-deposited diamond, the long-term cycling between 0 and 2.3 V was carried out, and the stability for the ECL reaction in the high potential range was also examined. One thousand cycles were performed at a sweep rate of 50 mV s^{-1} . Figure 9 shows a series of voltage–ECL curves recorded during the cycling period. For the GC electrode (Figure 9B), there is the progressive decrease of ECL peak intensity at 1.2 V with cycle number. The ECL peak intensity prior to cycling is $12.7 \mu\text{A cm}^{-2}$ and decreased significantly to $2.9 \mu\text{A cm}^{-2}$ after cycling, representing a decrease of over 77%. In contrast, for the as-deposited diamond electrode (Figure 9A), it is clear that the change of the voltammetric feature was quite small, indicating higher stability for the ECL reaction than that for GC despite the same ECL route (direct oxidation route).

Figure 10 compares the change of the ECL peak intensities with cycle number for three electrodes. For an as-deposited diamond electrode, the relative intensities for both the first and second ECL are almost constant (ca. 0.91). In contrast, the relative intensity for GC is exponentially decreased with cycle number, reaching 0.23 at the end of the cycling. Therefore, the decreasing rate for the GC electrode is about 3 times higher than that for the as-deposited diamond. For polycrystalline Pt, the relative intensity decreased linearly with increase in the cycle number, and reached 0.35 at the end of the cycling. The possible explanation for the fouling of the ECL emission is the adsorption

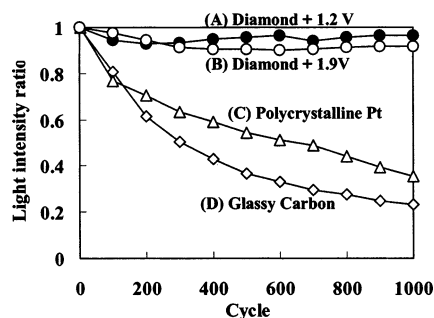


Figure 10. Relationship of the relative ECL peak intensity and the number of the potential cycling: the ECL peak at (A) 1.2 V and (B) 1.9 V vs Ag/AgCl for (a) the as-deposited diamond electrode; (C) the ECL peak at 1.2 V vs Ag/AgCl for the polycrystalline Pt electrode; (D) the ECL peaks at 1.2 V vs Ag/AgCl for the GC electrode.

of the reaction products.^{45,46} As the ECL process for both the second peak at the diamond and the GC electrodes are thought to be identical, then the high stability for the ECL at diamond may be due to the low adsorption properties for the reaction product. It might be also due to the oxidation decomposition for adsorption species at very high over-potentials. Moreover, at the GC electrode, the degree of the fouling was supposed to be higher than that for Pt due to a large number of reaction products (secondary and primary amines) through the direct TPrA oxidation compared to catalytic TPrA oxidation.

This result indicates a clear difference of the stability of the ECL reaction between the as-deposited diamond electrode and for the conventional electrodes (GC and polycrystalline Pt). In conclusion, the diamond appears a very promising electrode for the analytical electrochemical detector using the $\text{Ru}(\text{bpy})_3^{3+}$ chemiluminescent system that enables the detection of the primary amines with high efficiency and exhibits high stability.

Conclusions

For $\text{Ru}(\text{bpy})_3^{2+}$ /amines system, at the as-deposited diamond electrode, the anodic potential limit for the electrogenerated chemiluminescence (ECL) emission was 2.5 V vs Ag/AgCl due to the wide potential window in the aqueous solution. This potential range is remarkably wider than those for the GC and polycrystalline Pt electrodes, resulting in the detection of ECL for amines with higher oxidation potentials. Moreover, the complicated ECL routes were separated by using the diamond electrode due to the difference of the electrochemical activity for the direct amines oxidation at the electrode surface.

The ECL process of the $\text{Ru}(\text{bpy})_3^{2+}$ /co-reactant system has two routes to generate the oxidized form of co-reactant which play an important role in generating the excited state of $\text{Ru}(\text{bpy})_3^{2+*}$. One route is the homogeneous electron transfer between ruthenium and amine (catalytic route), and another route is the direct oxidation of amine at the electrode. However, at a conventional electrode, i.e., polycrystalline Pt and GC, these routes could not be clearly separated because the oxidation potentials of $\text{Ru}(\text{bpy})_3^{2+}$ and amines are very close. At the as-deposited diamond electrode, these two oxidation potentials were separated by ca. 500 mV. This potential difference enables us to show clear separation for each ECL route. Moreover, the successive dealkylation reaction and the ECL reaction through the direct oxidation for the dealkylation products (secondary and primary amines) could be observed. Anodic oxidation of primary amine in aqueous solution is difficult with GC or polycrystalline Pt electrodes due to the limited potential (oxygen evolution). However, by using the diamond electrode, even for primary amines i.e., methylamine (MA) or ethylamine (EtA)

with very high oxidation potentials, the direct oxidation potential could be detected through the ECL process. These results indicate that the diamond electrode can be applied to the electrochemical detector using the $\text{Ru}(\text{bpy})_3^{3+}$ chemiluminescent system for primary amines.

In the impedance measurements, the difference of the electrochemical behavior in each ECL process could also be identified. For a catalytic route, the impedance plots trace a semicircle connected with a 45 degree line. This process corresponds to the outer-phase electron-transfer reaction controlled by the diffusion of $\text{Ru}(\text{bpy})_3^{2+}$. For the direct oxidation route, the impedance plots trace two defused semicircles, suggesting that the capacitance component includes the constant phase element. The larger degree of the deformation of the semicircle at GC than that for diamond indicates the higher adsorption for the oxidation product. For the purpose of analytical application, stability of the ECL reaction is important. At the as-deposited diamond electrode, the light intensity exhibited a stable behavior during 1000 potential cycling. The decrease of the light intensity was only ca. 0.1 of the initial intensity. The high stability is attributable to the low adsorption property for reaction products.

We could demonstrate the detection for the compound with higher oxidation potential with high stability using a diamond electrode and the ECL reaction, suggesting that the diamond is the promising candidate for the electrode material for analytical application using ECL. At high potentials (i.e., 2.3 V vs Ag/AgCl), many amines might be directly oxidized at the electrode surface. Therefore, for the separate detection of the primary amine (i.e., methylamine), this system should be adapted as an HPLC postcolumn detector. This HPLC system is under development. Amino acids and oxalic acid are known as co-reactants in the $\text{Ru}(\text{bpy})_3^{2+}$ system that could exhibit the ECL emission. Amino acids, after derivatization and HPLC separation, are commonly monitored by use of UV, fluorescence, electrochemical, or chemiluminescence detection at low potential range. To develop the high sensitivity and easier separate detection for the amino acid, it is useful to adopt the ECL detector using the diamond electrode as an HPLC postcolumn detector, because of the high sensitivity at a higher potential region. Moreover, the simple measurement system for oxalic acid in urine can also be developed by using the $\text{Ru}(\text{bpy})_3^{2+}$ modified diamond electrode.

Acknowledgment. This research was supported by the Japan Society for the Promotion of Science (JSPS) Research for the Future Program (Exploratory Research on Novel Materials and Substances for Next-Generation Industries).

References and Notes

- (1) Martin, H. B.; Argoitia, A.; Landau, U.; Anderson, A. B.; Angus, J. C. *J. Electrochem. Soc.* **1996**, *143*, L133.
- (2) Swain, G. M.; Anderson, A. B.; Angus, J. C. *MRS Bull.* **1998**, *23*, 56.
- (3) Wu, Z. Y.; Yano, T.; Tryk, D. A.; Hashimoto, K.; Fujishima, A. *Chem. Lett.* **1998**, 503.
- (4) Swain, G. M. *J. Electrochem. Soc.* **1994**, *141*, 3382.
- (5) Honda, K.; Rao, T. N.; Tryk, D. A.; Fujishima, A.; Watanabe, M.; Yasui, K.; Masuda, H. *J. Electrochem. Soc.* **2000**, *147*, 659.
- (6) Honda, K.; Rao, T. N.; Tryk, D. A.; Fujishima, A.; Watanabe, M.; Yasui, K.; Masuda, H. *J. Electrochem. Soc.* **2001**, *148*, A668.
- (7) Yoshimura, M.; Honda, K.; Uchikado, R.; Kondo, T.; Rao, T. N.; Tryk, D. A.; Fujishima, A.; Masuda, H. *Diamond Relat. Mater.* **2001**, *10*, 620.
- (8) Fryda, M.; Herrmann, D.; Schater, L.; Klages, C.-P.; Perret, A.; Haenni, W.; Comninellis, C.; Gandini, D. *New Diamond Frontier Technol.* **1999**, *9*, 3.

- (9) Okino, F.; Shibata, H.; Kawasaki, S.; Touhara, H.; Morita, K.; Nishitani, M. G.; Sakaguchi, I.; Ando, T. *Electrochem. Solid-State Lett.* **1999**, *2*, 8.
- (10) Wang, J.; Swain, G. M.; Tachibana, T.; Kobayashi, K. *Electrochem. Solid-State Lett.* **2000**, *3*, 286.
- (11) Honda, K.; Yoshimura, M.; Rao, T. N.; Tryk, D. A.; Fujishima, A.; Yasui, K.; Sakamoto, Y.; Nishio, K.; Masuda, H. *J. Electroanal. Chem.* **2001**, *514*, 35.
- (12) Wang, J.; Swain, G. M. *Electrochem. Solid-State Lett.* **2002**, *5*, E4.
- (13) Rao, T. N.; Fujishima, A. *Diamond Relat. Mater.* **2000**, *9*, 3.
- (14) Granger, M. C.; Swain, G. M. *J. Electrochem. Soc.* **1999**, *146*, 12.
- (15) Popa, E.; Notsu, H.; Miwa, T.; Tryk, D. A.; Fujishima, A. *Electrochem. Solid-State Lett.* **1999**, *2*, 49.
- (16) Yoo, K.; Millar, B.; Kalish, R.; Shi, X. *Electrochem. Solid-State Lett.* **1999**, *2*, 233.
- (17) Uchikado, R.; Rao, T. N.; Tryk, D. A.; Fujishima, A. *Electrochem. Solid-State Lett.* **2001**, 144.
- (18) Noffsinger, J. B.; Danielson, N. D. *Anal. Chem.* **1987**, *59*, 865.
- (19) Lee, W.-Y.; Nieman, T. A. *Anal. Chem.* **1995**, *67*, 1789.
- (20) Blackburn, G. F.; Shah, H. P.; Kenten, J. H.; Leland, J.; Kamin, R. A.; Link, J.; Perterman, J.; Powell, M. J.; Shah, A.; Telly, D. B.; Tyagi, S. K.; Wilkins, E.; Wu, T.-G.; Massey, R. J. *Clin. Chem.* **1991**, *37*, 1534.
- (21) Yano, T.; Tryk, D. A.; Hashimoto, K.; Fujishima, A. *J. Electrochem. Soc.* **1998**, *145*, 1870.
- (22) Nostu, H.; Yagi, I.; Tatsuma, T.; Tryk, D. A.; Fujishima, A. *J. Electroanal. Chem.* **2000**, *429*, 31.
- (23) Leland, J. K.; Powell, M. J. *J. Electrochem. Soc.* **1990**, *137*, 3127.
- (24) Zu, Y.; Bard, A. J. *Anal. Chem.* **2000**, *72*, 3223.
- (25) Rubinstein, I.; Bard, A. J. *J. Am. Chem. Soc.* **1981**, *103*, 512.
- (26) Nicholson, R. S.; Shain, I. *Anal. Chem.* **1964**, *36*, 706.
- (27) Polcyn, D. S.; Shain, I. *Anal. Chem.* **1966**, *38*, 376.
- (28) Mann, C. K. *Anal. Chem.* **1964**, *36*, 2424.
- (29) Masui, M.; Sayo, H.; Tsuda, Y. *J. Chem. Soc. (B)* **1968**, 973.
- (30) Portis, L. C.; Bhat, V. V.; Mann, C. K. *J. Org. Chem.* **1970**, *35*, 2175.
- (31) Lias, S. G.; Bartmess, J. E.; Holmes, J. L.; Levin, R. D.; Liebman, J. F.; Mallard, W. G. Gas-Phase Ion and Neutral Thermochemistry. *J. Phys. Chem. Ref. Data* **1988**, *17*, Suppl., 1.
- (32) Kanoufi, F.; Zu, Y.; Bard, A. J. *J. Phys. Chem. B* **2001**, *105*, 210.
- (33) Koppang, M. D.; Witek, M.; Blau, J.; Swain, G. M. *Anal. Chem.* **1999**, *71*, 1188.
- (34) Bard, A. J.; Faulkner, L. R. *Electrochemical Methods*; Marcel Dekker: New York, 2001; Chapter 1.
- (35) Bard, A. J.; Menning, R.; Miller, B. *Pure Appl. Chem.* **1991**, *63*, 569.
- (36) Yilmaz, H.; Yurtsever, E.; Toppare, L. *J. Electroanal. Chem.* **1989**, *261*, 105.
- (37) Pysh, E. S.; Yang, N. C. *J. Am. Chem. Soc.* **1963**, *85*, 2124.
- (38) Akbulut, U.; Toppare, L.; Turker, L. *J. Polym. Sci. Polym. Chem.* **1985**, *23*, 1631.
- (39) Tani, T. *Photogr. Sci. Eng.* **1970**, *14*, 421.
- (40) Steffen, L. K.; Plummer, B. F.; Breley, T. L.; et al. *J. Phys. Org. Chem.* **1997**, *10*, 623.
- (41) Wu, X.; Mu, L.; Zhang, W. *J. Electroanal. Chem.* **1993**, *352*, 295.
- (42) Pajkossy, T. *J. Electroanal. Chem.* **1994**, *364*, 111.
- (43) Conway, B. E.; Bockris, J. O.; White, R. E. *Modern Aspects of Electrochemistry*, No. 32; Kluwer Academic/Plenum Publisher: New York, 1999; Chapter 2.
- (44) Schrebler, R.; Gomez, H.; Cordova, R.; Gassa, L. M.; Vilche, J. R. *Synth. Met.* **1998**, *93*, 187.
- (45) Xu, J.; Chen, Q.; Swain, G. M. *Anal. Chem.* **1998**, *70*, 3146.
- (46) Hubbard, A. T. *Chem. Rev.* **1988**, *88*, 633.